

PAPER • OPEN ACCESS

# Shape coexistence studied in $^{182,184}\text{Hg}$ via the $\beta$ decay of $^{182,184}\text{Tl}$

To cite this article: E Rapisarda *et al* 2017 *J. Phys. G: Nucl. Part. Phys.* **44** 074001

View the [article online](#) for updates and enhancements.

## Related content

- [-decay study of  \$^{182,184}\text{Tl}\$](#)   
C Van Beveren, A N Andreyev, A E Barzakh *et al.*
- [New systematic features in the neutron-deficient Au isotopes](#)  
M Venhart, J L Wood, M Sedláč *et al.*
- [Structure of  \$^{191}\text{Pb}\$  from  \$\alpha\$ - and  \$\beta\$ -decay spectroscopy](#)  
T E Cocolios, A N Andreyev, S Antalic *et al.*

# Shape coexistence studied in $^{182,184}\text{Hg}$ via the $\beta$ decay of $^{182,184}\text{Tl}^*$

E Rapisarda<sup>1,2</sup>, A N Andreyev<sup>3</sup>, S Antalic<sup>4</sup>, A Barzakh<sup>5</sup>,  
T E Cocolios<sup>1</sup>, I G Darby<sup>1</sup>, R De Groote<sup>1</sup>, H De Witte<sup>1</sup>,  
J Diriken<sup>1</sup>, J Elseviers<sup>1</sup>, D Fedorov<sup>5</sup>, V N Fedosseev<sup>6</sup>,  
R Ferrer<sup>1</sup>, M Huyse<sup>1</sup>, Z Kalaninová<sup>4</sup>, U Köster<sup>7</sup>, J Lane<sup>8</sup>,  
V Liberati<sup>8</sup>, K M Lynch<sup>9</sup>, B A Marsh<sup>6</sup>, P L Molkanov<sup>5</sup>,  
D Pauwels<sup>1</sup>, T J Procter<sup>10</sup>, D Radulov<sup>1</sup>, K Sandhu<sup>8</sup>,  
M D Seliverstov<sup>1</sup>, C Van Beveren<sup>1</sup>, P Van den Bergh<sup>1</sup>,  
P Van Duppen<sup>1</sup>, M Venhart<sup>11</sup>, M Veselský<sup>11</sup> and  
K Wrzosek-Lipska<sup>1,12</sup>

<sup>1</sup> KU Leuven, Instituut voor Kern- en Stralingfysica, B-3001, Leuven, Belgium

<sup>2</sup> Paul Scherrer Institut, Villigen, Switzerland

<sup>3</sup> Department of Physics, University of York, Heslington, York, YO10 5DD, United Kingdom

<sup>4</sup> Department of Nuclear Physics and Biophysics, Comenius University, 84248 Bratislava, Slovakia

<sup>5</sup> Petersburg Nuclear Physics Institute, NRC Kurchatov Institute, 188350 Gatchina, Russia

<sup>6</sup> EN Department, CERN, CH-1211 Geneve 23, Switzerland

<sup>7</sup> Institute Laue Langevin, F-38042, Grenoble, France

<sup>8</sup> School of Engineering and Science, University of West Scotland, Paisley, PA1 2BE, United Kingdom

<sup>9</sup> PH Department, CERN, CH-1211 Geneve 23, Switzerland

<sup>10</sup> School of Physics and Astronomy, The University of Manchester, Manchester M13 9PL, United Kingdom

<sup>11</sup> Slovak Academy of Sciences, Bratislava, SK-84511, Slovakia

<sup>12</sup> Heavy Ion Laboratory, University of Warsaw, PL-02-093 Warsaw, Poland

E-mail: [elisa.rapisarda@psi.ch](mailto:elisa.rapisarda@psi.ch)

Received 5 December 2016, revised 3 April 2017

Accepted for publication 6 April 2017

Published 31 May 2017



CrossMark

## Abstract

The  $\beta^+$ /EC decay of  $^{182,184}\text{Tl}$  to excited states in the daughter nuclei  $^{182,184}\text{Hg}$  has been investigated at the CERN on-line isotope mass separator facility. In both Tl nuclei two  $\beta$ -decaying states were observed. In the case of  $^{184}\text{Tl}$ , narrow-band laser spectroscopy could be used to disentangle the decay of both

\* This article belongs to the Focus on Exotic Beams at ISOLDE: A Laboratory Portrait special issue.



isomers. In  $^{182}\text{Hg}$  a precise energy of 335 (1) keV for the  $0_2^+$  state was measured together with its feeding from a tentatively proposed  $2_3^+$  state at 973 keV. Large conversion coefficients for the  $2_2^+ \rightarrow 2_1^+$  transition in  $^{182,184}\text{Hg}$  were measured to be 7.2 (13) and 14.2 (36), respectively, evidencing a strong E0 component.

Keywords: radioactive nuclei, shape coexistence,  $\beta$  decay,  $\gamma$  spectroscopy

(Some figures may appear in colour only in the online journal)

## 1. Introduction

The region of neutron-deficient nuclei in the vicinity of the proton shell-gap at  $Z = 82$  and neutron mid-shell at  $N = 104$  exhibits conceivably the most extensive manifestation of shape coexistence, whereby a nucleus shows two (or more) distinct types of deformation at low energy. The coexistence of different deformations in the neutron-deficient mercury isotopes has been well established by using several techniques: from optical pumping and laser spectroscopy, to in-beam and decay spectroscopy. For a recent survey on the experimental data and the progress in the theoretical description we recommend [1]. However, in order to fully characterize in the Mercury nuclei the underlying link between collective features and their microscopic origin it is necessary to complete the experimental information on the yrast and non-yrast states with not only energies, but also branching rates, life times, static and transitional moments. Recent experiments, such as Coulomb excitation of radioactive Hg isotopes [2], lifetime measurements [3, 4], Tl  $\beta$ -decay studies [5] and laser-spectroscopy studies [6] are pursuing these goals.

In the case of even–even nuclei, shape coexistence manifests itself through the occurrence of  $0^+$  states, with distinctive bands built on top of them. In the even- $A$  neutron-deficient mercury isotopes the states associated with a weakly deformed, presumably oblate, ground state ( $\beta_2 \sim -0.15$ ) show an almost constant excitation behavior as a function of the neutron number while a parabolic intrusion of strongly deformed states associated with a presumably prolate band ( $\beta_2 \sim 0.25$ ) is observed, see figure 1 in [5]. A recent Coulomb-excitation study of even- $A$   $^{182-188}\text{Hg}$  fixes the oblate character of their ground state and establishes a larger deformation for the excited  $0^+$  state [2], while recent in-source laser-spectroscopy studies on the even Hg nuclei [6] extend the trend of a weakly deformed ground state down to  $^{178}\text{Hg}$ .

In an  $\alpha$ -decay study of  $^{186}\text{Bi}$  [7], two long-living states were identified in  $^{182}\text{Tl}$ : one fed in the decay of the 9.8 ms  $^{186m1}\text{Bi}$  and other fed in the decay of the 14.8 ms  $^{186m2}\text{Bi}$ . The relative positions of the isomers in  $^{186}\text{Bi}$  and  $^{182}\text{Tl}$  could not be obtained and no spin and parity suggestions were given. A  $\beta$ -decay study of  $^{182}\text{Tl}$  performed at ISOLDE [8] showed the population of the  $8^+$  state in  $^{182}\text{Hg}$  suggesting spin  $I = (7)$  for the  $\beta$ -decaying state of  $^{182}\text{Tl}$ . The half-life was measured to be 3.1(10) s. Next to  $\beta$  decay,  $^{182}\text{Tl}$  has also a weak  $\alpha$ -decay branch [9] having an half-life of 2.8(6) s [10]. In our  $\alpha$ -decay study [11] a more precise half-life of 1.9(1) s was obtained together with a lower limit of 0.49% for the  $\alpha$ -branching ratio. In our laser spectroscopy study [12] a spin  $I = (4)$  was tentatively assigned to the 1.9 s  $\alpha$ - and  $\beta$ -decaying state. In the same study a spin  $I = (7)$  was confirmed for the second  $\beta$ -decaying state.

In earlier studies on  $^{184}\text{Tl}$ ,  $\alpha$  as well as  $\beta$  decay has been observed with a respective half-life of 10(2) s [13] and 11(1) s [14]. The  $\beta$ -decay study showed feeding up to the  $8^+$  level in  $^{184}\text{Hg}$  suggesting a spin  $I = (7^+)$  for the  $\beta$ -decaying state but also strong  $\beta$  feeding was

observed to the first  $2^+$  state suggesting the existence of two  $\beta$ -decaying states with a similar half-life. In a further  $\alpha$ -decay study of  $^{188}\text{Bi}$  [15], three long-living states were identified in  $^{184}\text{Tl}$  having as possible spin:  $(10^-)$ ,  $(7^+)$  and  $(2^-)$ . In our internal-decay study of the  $(10^-)$  state in  $^{184}\text{Tl}$  [16], a half-life of 47.1(7) ms was measured together with a 506.1(1) keV excitation energy above the  $(7^+)$  isomer. In our  $\alpha$ -decay study [11],  $\alpha$ -decay branching ratios of 0.089 (19)%, 0.047(6)% and 1.22(30)% have been deduced for the  $(10^-)$ ,  $(7^+)$  and  $(2^-)$  states, respectively. A new half-life of 9.5(2) s was measured for the  $(2^-)$  state.

In this paper, which results from an extensive experimental program on neutron deficient Tl nuclei at ISOLDE, CERN, we report on the  $\beta$ -decay of  $^{182,184}\text{Tl}$  in which on-line mass separation is combined with resonant laser ionization (LI) to produce pure sources of  $^{182,184}\text{Tl}$ . This completes our decay study of these nuclei where the  $\alpha$ - and internal-decay parts have already been published [11, 16]. Also narrow-band lasers were used to probe the hyperfine splitting of the atomic states. These laser-spectroscopy studies will be published elsewhere [12] but in the case of  $^{184}\text{Tl}$  the narrow-band laser approach was used to enhance the production of the higher-spin isomers. The  $\beta$  decay of the involved isotopes and isomers feeds levels in  $^{182,184}\text{Hg}$  which are characterized through  $\beta$ - $\gamma$ ,  $e$ - $\gamma$  and  $\gamma$ - $\gamma$  coincidence studies.

## 2. Experimental setup

The two experiments (IS466 for  $^{182}\text{Tl}$  and IS511 for  $^{184}\text{Tl}$ ) were performed at CERN-ISOLDE and are part of a systematic  $\alpha$ -,  $\beta$ -,  $\beta$ -delayed fission and laser spectroscopy study of neutron-deficient thallium isotopes. In both experiments, the  $^{182,184}\text{Tl}$  radioactive ions were produced in a 1.4 GeV proton-induced spallation of a  $50\text{ g cm}^{-2}$   $\text{UC}_x$  target followed by surface and resonant LI [17] in a similar way as used for the study of  $^{180}\text{Tl}$  reported in [5]. The ions were subsequently extracted from the ion source, accelerated to 50 keV and separated according to their mass-to-charge ratio with the general purpose separator. As a result, a high-purity beam of  $^{182}\text{Tl}$  or  $^{184}\text{Tl}$  was obtained. The typical intensity of the  $^{182,184}\text{Tl}$  beams at the detection setup was in the order of  $10^4$  pps. The intensity of  $^{184}\text{Tl}$  was reduced in order to avoid saturating the data acquisition system.

The experimental setup and data acquisition system were identical for the two experiments. They are also described in [11, 16]. The thallium beam was implanted on one of ten carbon foils,  $20\text{ }\mu\text{g cm}^{-2}$  thick, set on a rotatable wheel inside a vacuum chamber. By rotating the wheel every 40–50 s, the irradiated foil was moved to the decay position and the next foil moved to the implantation position. Two silicon detectors were placed in close geometry at the implantation point, as shown in figure 1 in [18], covering a solid angle of 24% of  $4\pi$ . An annular detector (Si1) having an active area of  $450\text{ mm}^2$  and thickness  $300\text{ }\mu\text{m}$ , placed upstream the foil, has a central hole of 8 mm so that the ion beam was passing through this hole before being implanted into the foil. A circular detector (Si2) of active area  $300\text{ mm}^2$  and thickness  $300\text{ }\mu\text{m}$  was placed behind the foil. Two extra circular Si detectors,  $300\text{ }\mu\text{m}$  thick and  $300\text{ mm}^2$ , were placed at the decay position.

The Si detectors were used for the detection of electrons, positrons, and  $\alpha$ -rays. In this article we concentrate on positrons and conversion electrons. Due to the limited thickness, the Si detectors mainly acted as  $\Delta E$  detectors for the electrons and positrons yielding a  $\Delta E$  peak around  $\approx 250\text{ keV}$  (see the red curve in figure 1). However for conversion electrons in the energy range between 200 and 500 keV, the full energy could be observed (see figure 1). The full-energy detection efficiency of Si2 was determined by using the known 375 keV  $(0_2^+ \rightarrow$

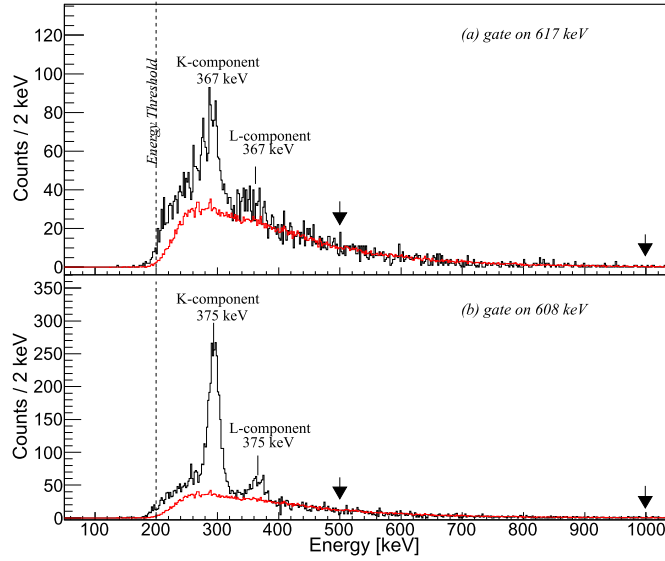


**Figure 1.** Si2 spectrum for  $A = 184$  gated on (a) the 617 keV ( $2_3^+ \rightarrow 2_1^+$ ) transition and (b) the 608 keV ( $2_3^+ \rightarrow 0_2^+$ ) transition in Ge1 and Ge2. The red curve shows the  $\Delta E$  background due to the  $\beta$  particles. The  $K$  and  $L$  electron lines of the 367 keV ( $2_1^+ \rightarrow 0_1^+$ )  $E2$  transition and 375 keV ( $0_2^+ \rightarrow 0_1^+$ )  $E0$  transition are indicated. The arrows indicate the energy range used to normalize the  $\beta$ -ray spectrum to the  $\gamma$ -ray-gated Si spectrum.

$0_1^+$ )  $E0$  transition in  $^{184}\text{Tl}$  [14]. In figure 1(b) the  $K$  and  $L$  electrons of this  $E0$  are shown through a coincidence with the feeding 608 keV transition. This yields an efficiency of 7.6 (16)% at 292 keV and 7.2(17)% at 360 keV. The red  $\Delta E$  curve in figure 1 is deduced from the Si spectra in coincidence with the 511 keV  $\gamma$  ray from the positron annihilation. Its normalization to the Si spectra gated on the 617 keV ( $2_3^+ \rightarrow 2_1^+$ ) transition (figure 1(a)) and 608 keV ( $2_3^+ \rightarrow 0_2^+$ ) transition (figure 1(b)) is based on matching the energy region between 500 and 1000 keV (see arrows in figures 1(a) and (b)). The  $\gamma$  rays following the de-excitation of the levels fed in the daughter nuclei were detected by two individual HPGe detectors placed outside the vacuum chamber at  $0^\circ$  (Ge1) and  $90^\circ$  (Ge2) with respect to the direction of the incoming beam. The typical energy resolution of each detector for a 1.3 MeV  $\gamma$  ray was  $\sim 3.1$  keV (FWHM). Energy and efficiency calibrations were performed using standard sources of  $^{133}\text{Ba}$ ,  $^{137}\text{Cs}$ ,  $^{60}\text{Co}$  and  $^{152}\text{Eu}$ . As explained in [11], the effective absolute efficiency of the HPGe detectors during the decay measurements is lowered with respect to the one determined from the calibration sources due to summing and loss effects related to the high  $\gamma$  multiplicity, the close-detector geometry and the count-rate. The efficiency for the 351 and 367 keV  $\gamma$  lines, the  $2_1^+ \rightarrow 0_1^+$  transitions in  $^{182}\text{Hg}$  and  $^{184}\text{Hg}$ , respectively, has been determined by  $\gamma$ - $\gamma$  coincidences. With this method an efficiency of 0.77(7)% and 0.44(4)% for the 351 keV line in  $^{182}\text{Hg}$  was obtained for Ge1 and Ge2, respectively, and 2.0(2)% and 0.71(7)% for the 367 keV line in  $^{184}\text{Hg}$ .

The difference in efficiency for the 351 keV in  $^{182}\text{Hg}$  and the 367 keV in  $^{184}\text{Hg}$  is due to the difference in count-rate. The effect of the multiplicity for the different  $\gamma$  lines within the same isotope was examined and could be ignored in the deduced intensities relative to the  $2^+ \rightarrow 0^+$  transition.

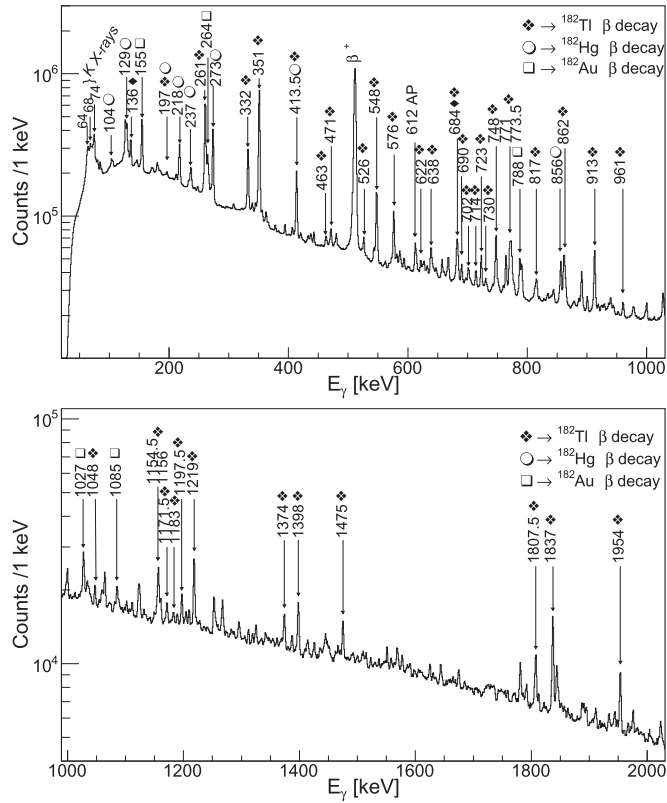


**Figure 2.**  $\gamma$ -ray singles spectrum obtained at  $A = 182$  by the Ge1 detector. Transitions assigned to the decay of  $^{182}\text{Tl}$  are indicated, together with some identified transitions belonging to daughter nuclei. The other lines are due to room background or residual radioactivity due to previous implantations. The numbers next to the peaks give the energies in keV.

### 3. Results

#### 3.1. The $\beta$ -decay of $^{182}\text{Tl}$

Narrow-band laser scans probing the hyperfine structure of  $^{182}\text{Tl}$  [12] were used to verify the proposed presence of two isomeric states [7]. A different hyperfine structure was observed when gating on  $\gamma$  rays de-exciting high-spin levels or on  $\gamma$ -rays de-exciting low-spin levels, yielding evidence for the existence of two  $\beta$ -decaying states. However, it was not possible to disentangle the two  $\beta$ -decay patterns with reasonable accuracy and therefore the results here are from the mixture of the two isomers.

Figure 2 shows a  $\gamma$ -ray spectrum measured with the Ge1 detector. The assignment of  $\gamma$  lines to the  $\beta$  decay of  $^{182}\text{Tl}$  is based on  $\gamma$ - $\gamma$  coincidences and on previously known transitions [3, 19]. A spectrum of  $\gamma$  rays observed in coincidence with the 351 keV ( $2_1^+ \rightarrow 0_1^+$ ) transition, the strongest transition in  $^{182}\text{Hg}$ , is shown in figure 3. Out of the  $\gamma$ - $\gamma$  coincidences a level scheme was constructed and for many weaker transitions the coincidence spectra were also used to determine relative intensities.

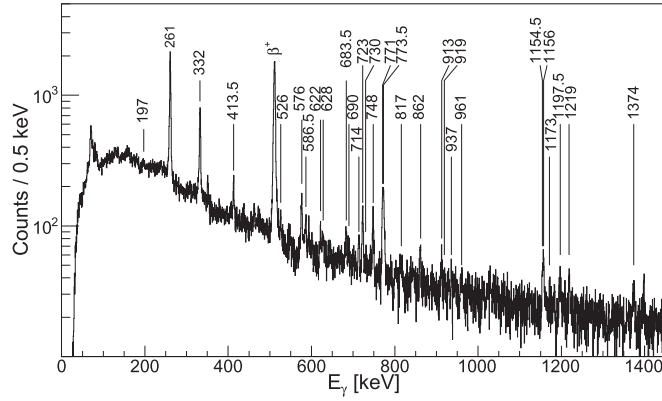


**Figure 3.** The  $\gamma$ -ray spectrum coincident with the 351 keV  $2_1^+ \rightarrow 0_1^+$  transition in  $^{182}\text{Hg}$ . The labels in the spectrum give the energy of the transitions in keV.

Table 1 summarizes the energy and intensities, relative to the 351 keV transition, of all the transitions identified in  $^{182}\text{Hg}$  in the present work, as well as the energy of the initial state and the coincident  $\gamma$  rays.

The resulting level scheme of  $^{182}\text{Hg}$  is shown in figure 4. The  $\beta$ -feeding intensities are based on the intensities from table 1 using the internal conversion coefficients for transitions where the multipolarity is known or deduced. The internal conversion coefficients are taken from [22], except for the conversion coefficient of the 197 keV  $\gamma$  line which was deduced here (see below). It should be noted that the  $\beta$ -decay feedings presented here are upper limits due to the lack of experimental sensitivity to low-intensity, high-energy  $\gamma$ -rays transitions leading to unobserved  $\gamma$ -ray feeding from high-lying states.

Many new levels and transitions have been identified in this work compared to the previous data [8, 19, 23, 24] obtained from in-beam and decay spectroscopy and the decay properties of several low-lying levels have been significantly improved. The most significant results, in relation to the investigation of the shape coexistence in Hg, are the precise energy determination of the  $0_2^+$  (335(1) keV) and its feeding together with the identification of a tentatively assigned ( $2_3^+$ ) state at 973 keV. Both states have been studied through  $e-\gamma$  coincidences.

The identification of the  $0_2^+$  at 328(12) keV in  $^{182}\text{Hg}$  was reported for the first time in [24] from the study of the fine-structure of the  $\alpha$  decay of  $^{186}\text{Pb}$ . In the singles Si spectrum, a strong electron line at 270(19) keV is present which intensity cannot be fully explained by the  $K$  conversion of the 351 keV  $2_1^+ \rightarrow 0_1^+$   $E2$  transition, indicating also here the presence of the  $0_2^+$  level through the  $K$  electrons of its  $E0$  decay. By inspecting, in figure 5, the  $\gamma$  rays coincident with these electrons, the transitions at 213, 576, 638, 702 and 748 keV can be attributed to a decay pattern feeding the  $0_2^+$  state while the 261 keV  $\gamma$  line is the  $4_1^+ \rightarrow 2_1^+$  transition in coincidences with conversion electrons from the intense 351 keV  $2_1^+ \rightarrow 0_1^+$  transition. By looking to the events in the Si2 detector in coincidence with the 638 keV transition, see figure 6(b), the electron peak is at 250(14) keV, leading to an  $E0$  transition of 330(14) keV in agreement with the value of 328(12) keV reported in [24].

Finally the  $\gamma$  rays observed in coincidence with the 638 and 213 keV transitions lead to the placement of these lines in the level scheme and thus fix the energy of the  $0_2^+$  state at 335 (1) keV. The 638 keV line de-excites the level at 973 keV, a candidate for the  $2_3^+$  state (see further in the Discussion section).

**Table 1.** The  $\gamma$ -ray energy,  $\gamma$ -ray intensity relative to the transition at 351 keV, energy of the initial state and observed coincident  $\gamma$  rays for the transitions belonging to the  $\beta$  decay of  $^{182}\text{Tl}$ . The  $\gamma$ -ray intensities are determined from the  $\gamma$  singles spectrum, unless otherwise indicated.

Energy (keV)	Relative $\gamma$ -ray intensity (%)	Initial level (keV)	Observed coincident $\gamma$ rays (keV)
196.7(10)	1.6(5)	547.9	
213(1)	0.9(3) <sup>a</sup>	547.9	
260.8(6)	61.5(18) <sup>b</sup>	611.9	332.4, 351.1, 413.5, 463.0, 586.5, 683.5, 770.7, 817.0, 862.1, 919.0, 936.6, 1154.5, 1373.8, 1398.2, 1475.0, 1807.5, 1837.2, 1953.7
332.4(6)	23.9(4)	944.3	260.8, 351.1, 413.5, 586.5, 817.0, 862.1, 1398.2, 1475.0
351.1(6)	100	351.1	196.7, 260.8, 332.4, 406.8, 413.5, 463.0, 547.9, 576.4, 586.5, 621.9, 683.5, 714.0, 723.1, 747.9, 770.7, 773.5, 862.1, 913.0, 1156.2, 1218.6, 1373.8, 1398.2, 1475.0, 1807.5, 1837.2, 1953.7
378.1(6)	1.3(5)	1761.0	260.8, 351.1, 770.7
406.8(9)	2.3(1)	1531.0	351.1, 547.9, 576.4, 773.5
413.5(6)	3.0(6) <sup>b</sup>	1357.8	260.8, 332.4, 351.1
463.0(9)	2.8(1)	1074.4	260.8, 351.1
471.0(6)	4.9(1)	1766.5	260.8, 351.1, 547.9, 683.5, 747.9
526.3(9)	2.4(1)	1074.4	351.1, 547.9, 714.0
547.9(6)	21.7(6)	547.9	406.8, 471.0, 526.3, 576.4, 747.9, 862.1, 913.0, 1218.6
576.4(6)	15.0(5)	1124.4	196.7, 351.1, 406.8, 547.9, 862.1, 913.0, 1218.6
586.5(9)	3.8(2)	1531.0	260.8, 332.4, 351.1
621.9(6)	1.8(4) <sup>b</sup>	972.9	351.1, 701.7
627.9(9)	2.2(7) <sup>b</sup>	2010.5	260.8, 351.1, 770.7
632.2(9)	1.0(1)	2419.3	714.0
637.8(10)	1.9(6) <sup>b</sup>	972.9	701.7
683.5(9)	3.7(4) <sup>b,c</sup>	{ 1295.6 2449.9	260.8, 351.1, 471.0
690.1(6)	2.4(1)	1986.0	260.8, 351.1, 547.9, 683.5, 747.9
701.7(9)	2.5(1)	1674.7	621.9, 637.8
714.0(9)	2.0(1)	1788.4	351.1, 463.0, 526.3, 632.2, 723.1
723.1(6)	5.2(2)	1074.4	351.1, 714.0
730.3(9)	1.7(1)	2449.9	351.1, 547.9, 1172.6
747.9(6)	12.9(6)	1295.6	196.7, 351.1, 547.9, 471.0, 690.1, 1047.6
770.7(9)	7.3(7) <sup>b</sup>	1382.6	260.8, 351.1, 378.1, 627.9, 1036.6, 1182.8
773.5(9)	9.4(18) <sup>b</sup>	1124.4	351.1, 406.8, 862.1, 913.0, 1218.6
817.0(9)	1.3(3) <sup>b</sup>	1761.0	260.8, 332.4, 351.1
862.1(6)	7.2(11) <sup>b</sup>	1986.0	351.1, 547.9, 576.4, 773.5



**Table 1.** (Continued.)

Energy (keV)	Relative $\gamma$ -ray intensity (%)	Initial level (keV)	Observed coincident $\gamma$ rays (keV)
913.0(6)	2.7(5) <sup>b</sup>	2037.4	351.1, 547.9, 576.4, 773.5
919.0(9)	0.7(1)	1531.0	260.8, 351.1
936.6(9)	0.7(3) <sup>b</sup>	1548.6	260.8, 351.1
960.7(6)	1.5(1)	1508.3	351.1, 547.9
1036.6(9)	1.2(5) <sup>b</sup>	2419.3	770.7
1047.6(6)	0.9(1)	2342.9	260.8, 351.1, 547.9, 683.5, 747.9
1154.5(9)	2.6(4) <sup>b</sup>	1766.5	260.8, 351.1
1156.2(9)	4.3(4) <sup>b</sup>	1508.3	351.1
1172.6(10)	1.8(4) <sup>b</sup>	1720.5	351.1, 547.9, 730.3
1182.8(6)	0.5(1) <sup>b</sup>	2565.5	770.7
1197.5(6)	2.4(3) <sup>b</sup>	1547.6	351.1
1218.6(6)	4.3(5)	2342.9	351.1, 547.9, 576.4, 773.5
1373.8(6)	1.6(2)	1986.0	260.8, 351.1
1398.2(6)	2.9(4)	2342.9	260.8, 332.4, 351.1
1475.0(6)	1.8(3)	2419.3	260.8, 332.4, 351.1
1807.5(6)	2.7(6)	2419.3	260.8, 351.1
1837.2(6)	5.4(12)	2449.9	260.8, 351.1
1953.7(6)	2.5(6)	2565.5	260.8, 351.1

<sup>a</sup> Determined from the  $\gamma$ -ray spectrum in coincidence with the  $K$  electron of the  $(0_2^+ \rightarrow 0_1^+)E0$  transition.

<sup>b</sup> Determined from  $\gamma$ - $\gamma$  coincidences.

<sup>c</sup> Multiply placed; undivided intensity is given.

In the recent study on  $^{180}\text{Hg}$  [5], the transition between the second and the first  $2^+$  states was found to have a large  $E0$  component ( $\alpha_{\text{ICC}} = 3.5(4)$ ). The possibility for a  $E0$  component of the 197 keV  $2_2^+ \rightarrow 2_1^+$  transition in  $^{182}\text{Hg}$  was investigated accordingly by inspecting the  $\gamma$ - $\gamma$  coincidences spectra with gates on the 576 keV and on the 748 keV transition. Both transitions feed the  $2_2^+$  state and allow to study the 197–351 keV  $\gamma$ -ray cascade. As shown in the  $\gamma$ - $\gamma$  coincidence spectrum gated on the 576 keV transition (figure 7), this transition is coincident with both the 548 keV and the 351 keV lines. The total transition intensity of the 197 keV transition ( $I_{\text{tot}} = 13.4(12)\%$ ) could be deduced by comparing the number of counts of the 548 and 351 keV peaks in the coincidences spectra with the 576 and 748 keV transitions. The total transition intensity of the 197 keV line is much larger than its relative  $\gamma$ -ray intensity of 1.6(5)% leading to a total internal conversion coefficient of  $(I_{\text{tot}} - I_{\gamma})/I_{\gamma} = 7.2(13)$ . The theoretical total electron conversion coefficients for a 197 keV  $M1$  and  $E2$  transition are 1.153 and 0.412, respectively [22]. The measured electron conversion implies that the 197 keV  $2_2^+ \rightarrow 2_1^+$  transition has a large  $E0$  component.

The weak  $2_2^+ \rightarrow 0_2^+$  213 keV transition was not observed in singles nor in the  $\gamma$ - $\gamma$  coincidence gate on the 576 keV; its intensity was deduced from its coincidence with the  $K$  electrons of the 335 keV  $E0$  in the Si detector (see figure 5).

### 3.2. The $\beta$ decay of $^{184}\text{Tl}$

Two different sets of data were collected with the aim to disentangle the decay scheme of the two  $\beta$ -decaying states. In the first data set no LI was used and only through surface ionization

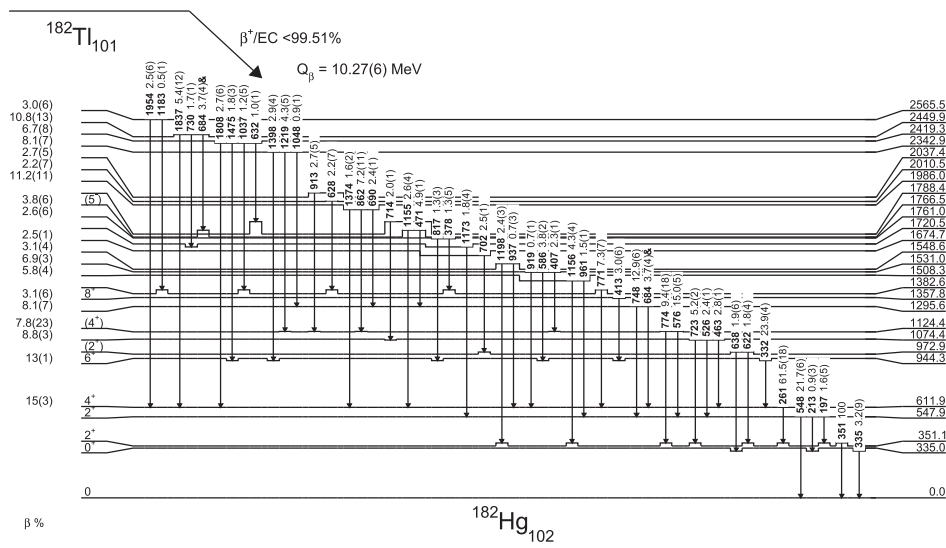


**Figure 4.** Level scheme of  $^{182}\text{Hg}$  deduced from the present work (energies in keV). The  $\gamma$ -ray intensities and the intensity of the 335 keV  $E0$  transition are normalized to the 351 keV ( $2_1^+ \rightarrow 0_1^+$ ) transition. The given  $\beta$ -feeding intensities are upper limits. Spin assignments are from NNDC [20] except for the ( $2^+$ ) assignment of the 973 keV level (see discussion in the next section). The  $Q_{EC}$  value comes from [21].

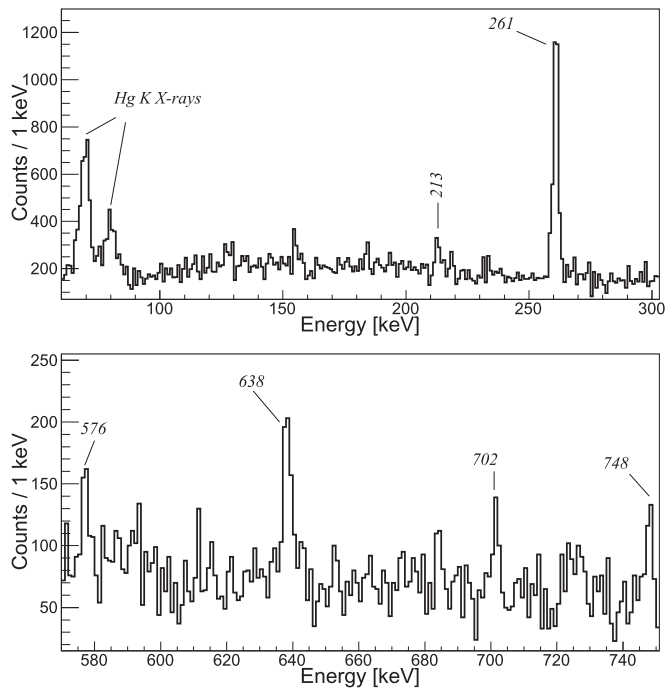


**Figure 5.** Part of the  $\gamma$ -ray spectrum in  $A = 182$ , background-subtracted, with a gate on the  $K$  electron of the  $0_2^- \rightarrow 0_1^-$   $E0$  transition in  $^{182}\text{Hg}$ . The top and bottom panels show the spectrum in a different energy range.

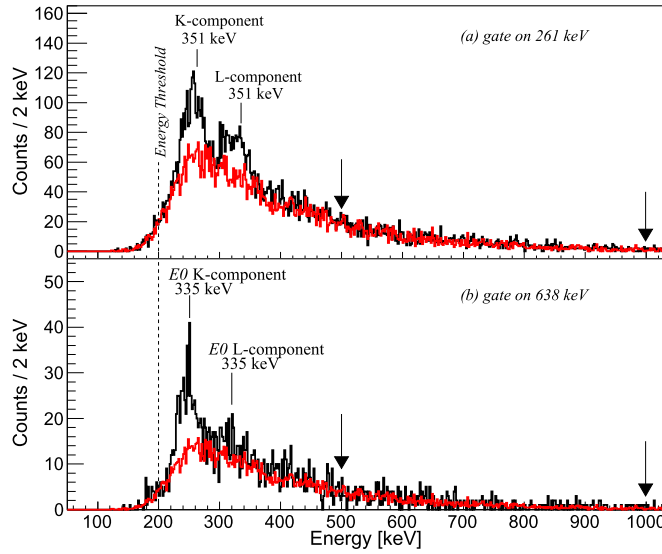


**Figure 6.** Si spectrum at  $A = 182$  gated on (a) the 261 keV transition and (b) the 638 keV transition. The red curve shows the  $\Delta E$  spectrum due to the  $\beta$  particles. The arrows indicate the energy range used to normalize the  $\beta$ -ray spectrum to the  $\gamma$ -gated Si spectrum.

(SI) a beam of  $^{184}\text{Tl}$  was obtained. This SI data set contains a mixture of the three long-lived states:  $(10^-)$ ,  $(7^+)$  and  $(2^-)$ .

In the second data set, further called as the LI data set, we made use of the in-source laser resonant ionisation technique in narrow bandwidth mode in order to enhance the production of the  $(10^-)$  isomer and consequently the production of the  $(7^+)$  state as the  $(10^-)$  isomer decays internally to the  $(7^+)$  state [15]. This was achieved by using a double-step excitation-ionisation laser scheme and tuning the first laser transition at a frequency of  $1/\lambda = 18058.75 \text{ cm}^{-1}$  before frequency doubling (see figure 1 and corresponding explanation in [16]). Information on the internal decay of the  $(10^-)$  isomer and on the  $\alpha$  decay of the different isomers are published, respectively, in [16, 11].

As the half-lives of the two  $\beta$ -decaying states of  $^{184}\text{Tl}$  are very similar, the  $\gamma$  rays belonging to one of the two decays could not be disentangled on the basis of their half-life behavior. However, by making use of the two data sets (laser off and laser on resonance to the  $(10^-)$ ), it became possible to deduce the origin of many transitions. This can be seen in figure 8 where two singles  $\gamma$ -ray spectra are shown, one in LI mode and one in SI mode, evidencing strong changes in relative intensity of a number of  $\gamma$  lines.

A so-called ‘pure’  $(7^+)$   $\beta$ -decay  $\gamma$ -ray spectrum, shown in figure 9(b), was obtained by using the LI data and subtracting the SI data normalized to the  $2_3^+ \rightarrow 0_2^+$  transition at 608 keV. Similarly, a pure  $(2^-)$  decay spectrum, shown in figure 9(a), was obtained by using the SI data and subtracting the LI data normalized to the  $6^+ \rightarrow 4^+$  transition at 340 keV. In this procedure we assumed that the  $2_3^+$  state and the  $6^+$  state could be only fed by the decay of  $(2^-)$  and  $(7^+)$  states in  $^{184}\text{Tl}$ , respectively. Furthermore, in order to remove the contribution of  $\gamma$  rays due to the 47 ms  $(10^-)$  internal decay, we selected only  $\gamma$  rays emitted after 200 ms following the proton impact on target. The described subtracting procedure was also applied to produce pure  $(2^-)$  and  $(7^+)$  Si spectra as well.

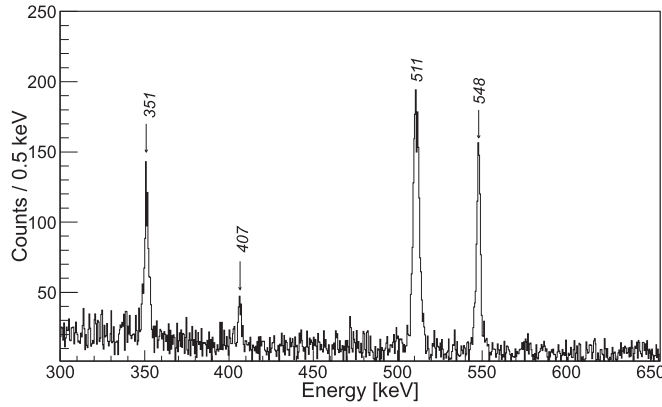


**Figure 7.** Part of the  $\gamma$ - $\gamma$  coincidence spectrum in  $A = 182$  with a gate on the 576 keV transition.

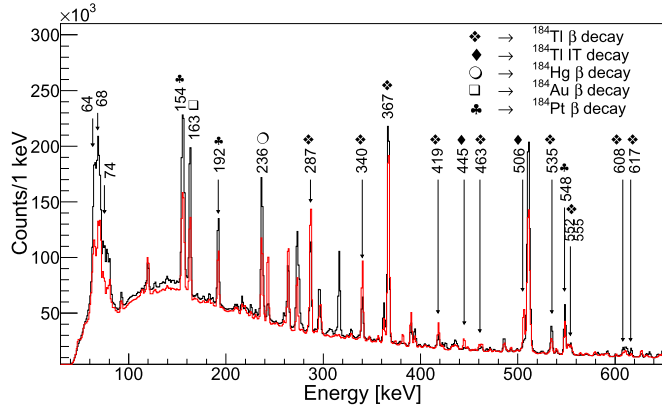


**Figure 8.** Singles  $\gamma$ -ray spectra detected by Ge1 at mass  $A = 184$ . Red line: LI data; black line: SI data. The SI spectrum is scaled by a factor 0.5.

In the rest of the text and for simplicity, we will refer to the two subtracted spectra as the pure  $(2^-)$  and the pure  $(7^+)$  spectrum.

All  $\gamma$  transitions attributed to the decay of  $^{184}\text{Tl}$  ( $7^+$ ) and  $(2^-)$  states are listed in table 2 with energies and relative  $\gamma$ -ray intensities. The intensities of the  $\gamma$  rays were calculated from the pure  $(2^-)$  and  $(7^+)$  singles- $\gamma$ -ray spectrum, where possible. For weak  $\gamma$  rays and  $\gamma$ -ray transitions contaminated by other decays than  $^{184}\text{Tl}$ , we made use of the branching ratios determined in the original SI and LI data sets.

In contrast to previous work [14] where only one decay scheme is presented, two decay schemes can be constructed (see figures 10(a) and (b)) involving many new levels. It is clear from the apparent feeding of 20(6)% of the  $2_1^+$  level in the decay of the  $(7^+)$  state that the assumptions used for producing the pure spectra are not completely fulfilled. As the  $Q_\beta$  value is high (9.46 MeV) and only levels in  $^{184}\text{Hg}$  up to 2.12 MeV are observed, there is quite room for unobserved  $\gamma$  rays from high-lying states, feeding the lowest states. Therefore the quoted  $\beta$ -feeding intensities are only upper limits.

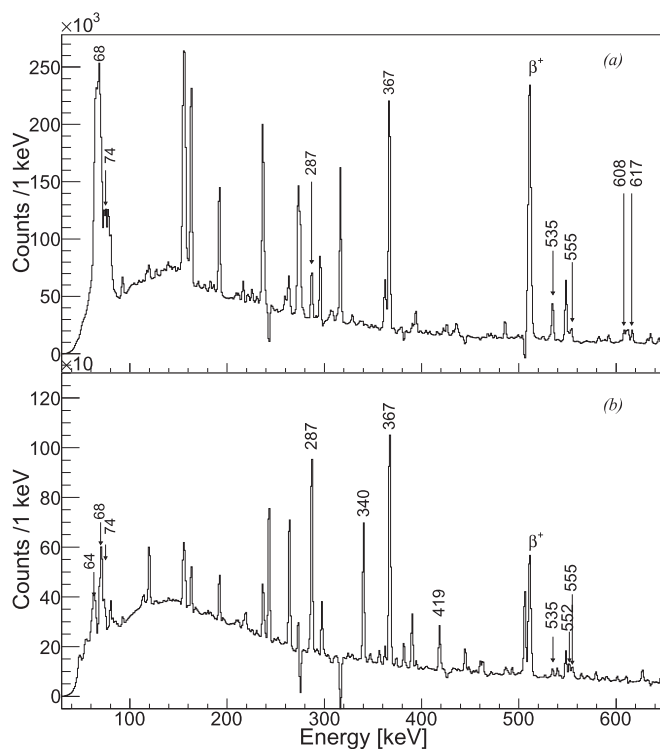


**Figure 9.** Singles  $\gamma$ -ray spectrum of a pure (a) ( $2^-$ ) decay and (b) ( $7^+$ ) decay in  $^{184}\text{Tl}$  from Ge1.

The relative intensity of the  $0_2^+ \rightarrow 0_1^+$  transition present in the  $^{184}\text{Tl}$  ( $2^-$ ) decay was determined by using the pure ( $2^-$ )  $\gamma$ -ray and Si spectra. The 375 keV,  $0_2^+ \rightarrow 0_1^+$ , and 367 keV,  $2_1^+ \rightarrow 0_1^+$ , transitions are very close in energy and therefore the  $K$ -electron peaks of the two transitions cannot be separated in the singles Si spectrum as they appear as one bump located around 290 keV. However, by comparing the Si spectrum gated by the 608 keV line (see figure 1(b)) with the Si spectrum gated by the 617 keV line (see figure 1(a)) and using the known conversion coefficient of the 367 keV  $2_1^+ \rightarrow 0_1^+$   $E2$  line, the 375 keV  $E0$  intensity can be obtained.

Also in  $^{184}\text{Tl}$  we investigated the possibility for a  $E0$  component in the 168 keV  $2_2^+ \rightarrow 2_1^+$  transition by intensity balance consideration. Figure 11 shows the spectrum of  $\gamma$  rays in coincidence with the 552 keV transition, the strongest  $\gamma$  ray feeding the  $2_2^+$  state. The spectrum shows, together with the peak corresponding to the 535 keV  $2_2^+ \rightarrow 0_1^+$  transition, a pronounced 367 keV  $2_1^+ \rightarrow 0_1^+$  transition, that can be only explained in terms of a very intense  $2_2^+ \rightarrow 2_1^+$  transition. Indeed a total transition intensity of 19.5(49)% of the 168 keV transition can be deduced by comparing the number of counts in the 535 and 367 keV peaks. Since the observed  $\gamma$ -ray intensity in the SI data set is only 1.4(3)%, the  $2_2^+ \rightarrow 2_1^+$  transition has a total conversion coefficient of  $(I_{\text{tot}} - I_\gamma) / I_\gamma = 14.2(36)$ . This is the largest value of conversion coefficient known in this mass region.

**Table 2.** The  $\gamma$ -ray energy, the energy of the initial state,  $\gamma$ -ray intensity relative to the  $2^+ \rightarrow 0^+$  transition at 367 keV, for the transitions belonging to the  $\beta$  decay of  $^{184}\text{Tl}$ . In the third and fourth columns, the  $\gamma$ -ray intensities determined from the original SI and LI data sets are reported. In the fifth and sixth columns the  $\gamma$ -ray intensities determined from the pure  $2^-$  and pure  $7^+$  spectra are given. The intensities are determined from the singles  $\gamma$ -ray spectrum, unless otherwise indicated. For the 375 keV line the intensity of the ( $0_2^+ \rightarrow 0_1^+$ ) transition is given.

Energy keV	Initial energy level keV	Intensity in %			
		Surface Ionization	Laser Ionization	$2^-$	$7^+$
118.8(10)	654.0	$\leq 0.3^a$	$\leq 0.5^a$	$\leq 0.2^b$	$\leq 0.6^b$
159.2(5)	534.8	0.24(13) <sup>c</sup>	—	0.34(18) <sup>b</sup>	—
168.3(5)	534.8	1.4(3) <sup>a</sup>	1.1(4) <sup>a</sup>	1.9(4) <sup>b</sup>	0.5(1) <sup>b</sup>
287.1(3)	654.0	33.2(12)	49.7(18)	16.6(7)	63.8(41)
324.6(5)	1413.6	0.85(3)	1.1(1)	—	1.6(3)
340.3(3)	994.3	15.3(5)	31.7(11)	—	44.9(22)
367.0(3)	367.0	100	100	100	100
375.5(10)	375.5	—	—	7.9(20) <sup>d</sup>	—
389.7(5)	1803.3	1.5(4) <sup>a</sup>	3.0(6) <sup>a</sup>	—	4.1(11)
418.6(3)	1412.8	6.0(2)	13.2(4)	—	17.6(9)
432.8(5)	1086.6	0.8(2) <sup>a</sup>	1.7(4) <sup>a</sup>	—	1.9(7)
435.3(5)	1089.1	0.9(2) <sup>a</sup>	0.4(3) <sup>a</sup>	1.9(6) <sup>b</sup>	—
462.8(5)	1549.4	2.2(1)	3.9(2)	—	5.3(6)
534.8(3)	534.8	15.1(5)	8.9(3)	21.0(11)	4.9(4)
551.7(5)	1086.6	5.2(8) <sup>a</sup>	8.0(13) <sup>a</sup>	—	10.8(26) <sup>b</sup>
554.2(5)	1089.1	5.5(9) <sup>a</sup>	5.1(10) <sup>a</sup>	11.1(5)	—
555.4(3)	1549.4	1.6(2) <sup>a</sup>	2.8(3) <sup>a</sup>	—	3.8(6) <sup>b</sup>
608.2(3)	983.8	3.7(25) <sup>a</sup>	1.5(10) <sup>a</sup>	5.7(39) <sup>b</sup>	—
616.8(3)	983.8	4.9(2)	2.0(1)	7.6(4)	—
644.1(3)	1179.2	3.2(3) <sup>a</sup>	1.3(5) <sup>a</sup>	4.6(3)	—
646.3(3)	1300.3	1.4(2) <sup>a</sup>	2.2(3) <sup>a</sup>	0.8(1) <sup>b</sup>	2.3(4) <sup>b</sup>
649.5(5)	2063.4	0.9(2) <sup>a</sup>	1.7(2) <sup>a</sup>	—	2.6(5)
674.6(5)	1658.3	2.3(5)	1.0(2)	3.5(3)	—
709.3(5)	2122.1	2.9(2)	6.3(5)	—	8.2(10)
719.7(5)	1086.6	3.7(5) <sup>a</sup>	5.6(9) <sup>a</sup>	—	7.6(6)
722.0(5)	1089.1	3.4(5) <sup>a</sup>	2.5(8) <sup>a</sup>	3.3(6)	—
731.3(3)	1818.0	0.7(2) <sup>a</sup>	1.7(3) <sup>a</sup>	—	2.3(4)
754.6(3)	1738.4	1.3(3)	0.5(1)	1.9(2)	—
759.4(3)	1413.6	3.6(2) <sup>a</sup>	6.2(5) <sup>a</sup>	—	9.8(7)
765.6(3)	1300.3	3.9(2)	5.2(2)	2.4(2)	6.7(5)
803.4(5)	1179.2	0.5(2) <sup>c</sup>	0.2(1) <sup>c</sup>	0.7(4) <sup>b</sup>	—
809.1(5)	1803.3	0.9(2) <sup>a</sup>	2.2(3) <sup>a</sup>	—	3.8(6)
813.0(5)	1179.2	1.7(3) <sup>a</sup>	0.8(3) <sup>a</sup>	2.6(3)	—
878.3(3)	1872.6	0.5(1) <sup>a</sup>	1.1(4) <sup>a</sup>	—	1.5(7)
894.9(5)	1549.4	0.7(1) <sup>a</sup>	1.5(3) <sup>a</sup>	—	2.6(6)
915.2(5)	1450.0	1.2(3) <sup>a</sup>	0.6(3) <sup>a</sup>	2.5(2)	—
1083.0(5)	1450.0	0.8(3) <sup>a</sup>	0.4(3) <sup>a</sup>	1.3(3)	—
1179.2(5)	1179.2	1.9(1)	0.8(1)	2.9(2)	—

<sup>a</sup> Determined from  $\gamma$ - $\gamma$  coincidences.

<sup>b</sup> Deduced from the branching ratios determined in the original SI and LI data sets.

<sup>c</sup> Determined from the  $\gamma$ -ray spectrum with a gate on the  $K$  electron of the ( $0_2^+ \rightarrow 0_1^+$ )  $E0$  transition.

<sup>d</sup> Determined from the Si spectrum.

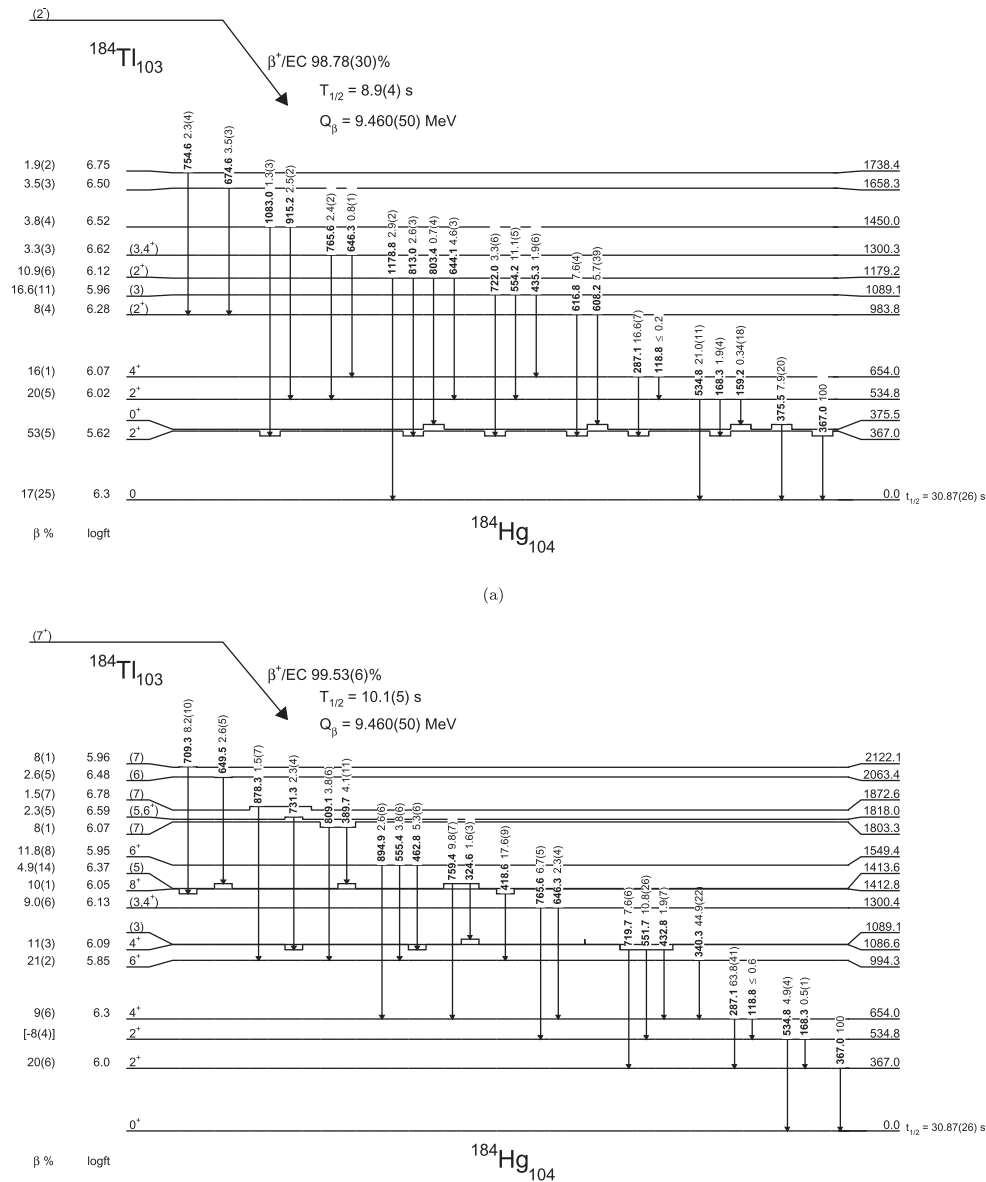


**Figure 10.** Decay scheme of the  $(2^-)$  (a) and  $(7^+)$  (b)  $\beta$ -decaying states in  $^{184}\text{Tl}$  deduced from the present work (energies in keV).  $\gamma$ -ray intensities are normalized to the 367 keV transition. The given  $\beta$ -feeding values are upper limits, implying that the  $\log ft$  values are lower limits. The half-life for the low-spin state is from our  $\alpha$ -decay study [11]. The half-life for the high-spin state is from the literature [25]. Spin assignments are from NNDC [25], except for the  $I = (3)$  assignment of the 1089 keV newly observed level (see discussion in the next session). The  $Q_{\text{EC}}$  value comes from [21].

#### 4. Discussion

The updated systematics of the lowest positive-parity states in the even-even  $^{180,182,184,186}\text{Hg}$  is shown in figure 12. With the precise determination of the energy of the  $0_2^+$  state in  $^{182}\text{Hg}$ ,

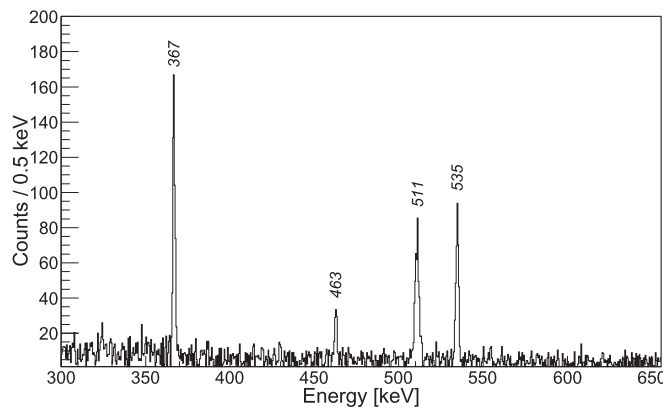


**Figure 11.** Part of the  $\gamma$ - $\gamma$  coincidence spectrum for  $A = 184$  with a gate on the 552 keV transition. The energy of the observed transitions is given in keV.

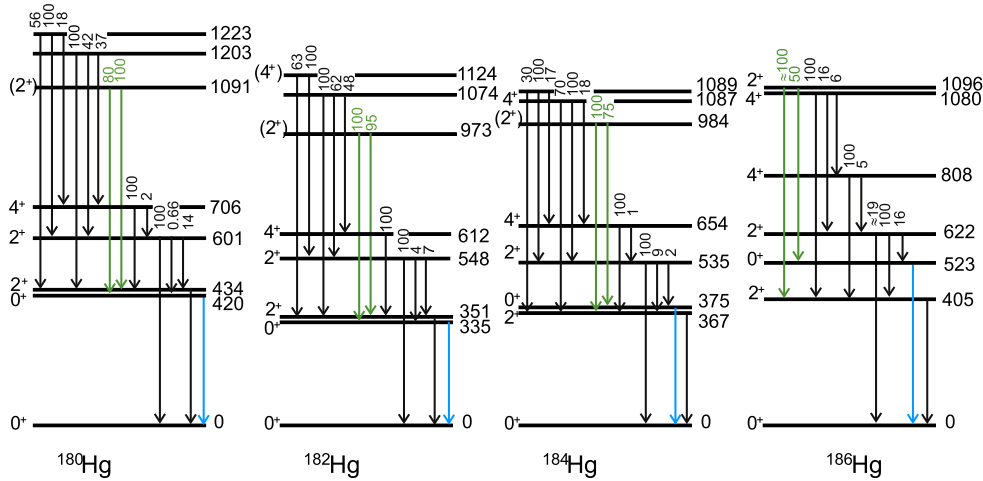


**Figure 12.** Systematic of the lowest positive parity states and their transitions in the even-even  $^{180,182,184,186}\text{Hg}$  nuclei. The green lines are the  $\gamma$  transitions of the possible  $\gamma$ -vibrational bandhead, i.e. the  $2_3^+$  state. The relative intensities and the spins are taken from the present work and [5, 20, 25, 31].

the energy systematic of the  $0_1^+$ ,  $0_2^+$ ,  $2_1^+$ ,  $2_2^+$  and  $4_1^+$  is completed. The identification of the 973 keV level in  $^{182}\text{Hg}$  completes the systematics of a level present in the four nuclei with a specific decay pattern, only feeding the  $0_2^+$ ,  $2_1^+$  levels, while no transition to the ground state is observed. This leads to the suggestion that it might be the  $(2^+)$  band-head of the  $\gamma$ -vibrational band built on top of the  $0_2^+$  deformed state [5, 14, 26].

Similarly to what has been observed in  $^{180}\text{Hg}$ , a doublet of states located at  $E^* \sim 1100$  keV is observed in  $^{182,184}\text{Hg}$ . The two states show a comparable decay pattern to the  $4_1^+$ ,  $2_2^+$ , and  $2_1^+$  states but it is unlikely that they have same spin and parity.

In  $^{182}\text{Hg}$ , the level at 1124.4 keV was placed on the basis of the 576.4 keV transition towards the  $2_2^+$  level with a possible transition to the  $2_1^+$  level and was interpreted as the  $4^+$



member of the oblate band [3]. In the present study the level is confirmed and also the transition to the  $2_1^+$  level is observed. The possible decay towards the  $4_1^+$  level could not be observed as its energy of 512.5 keV is too close to the 511 keV. The new level at 1074.4 keV was observed through its decay to the  $4_1^+$ ,  $2_2^+$ , and  $2_1^+$  levels.

In  $^{184}\text{Hg}$ , a level at 1086.6 keV was established in two in-beam experiments [27, 28] through the observation of the 552 keV transition to the  $2_2^+$  level and 720 keV transition to the  $2_1^+$  level and interpreted as the  $4^+$  member of the oblate band and also, according to NNDC [25] in the  $\beta$ -decay study of [14]. However, in the latter decay study the level lies at 1089 keV and the decay transitions are 554 and 722 keV. From the present study, it is clear that there are two levels and a level at 1089.1 keV is placed in the low-spin level scheme while in the high-spin decay scheme the level at 1089.1 keV is present next to a level at 1086.6 keV. The apparent  $\beta^+$ /EC feeding of the 1086.6 keV  $4^+$  level in the ( $7^+$ ) decay with a *logft* of 6.0 is most probably due to feeding through unobserved  $\gamma$  rays. The strong feeding of the 1089.1 keV level in the ( $2^-$ ) decay leads to a tentative (3) spin assignment.

Based on the relative  $\gamma$ -ray intensities (see figure 12), in both isotopes the assumed oblate  $4_2^+$  level decays favorably to the  $2_2^+$  state relative to the decay towards the  $2_1^+$  state, with a factor 6.9 for  $^{182}\text{Hg}$  and 5.4 for  $^{184}\text{Hg}$ . This can be understood by using the mixing amplitudes deduced in [2, 4] for the  $4^+$  and  $2^+$  states. The squares of the mixing amplitudes of the normal configuration of the  $4_2^+$  state are 97% and 96%, respectively in  $^{182}\text{Hg}$  and  $^{184}\text{Hg}$ , thus indicating a rather pure oblate character. The  $2^+$  states of the unperturbed bands are instead almost completely mixed giving a  $2_2^+$  state with 71% of the normal configuration in  $^{182}\text{Hg}$  and with 49% of the normal configuration in  $^{184}\text{Hg}$ .

The large conversion coefficient for the  $2_2^+$  to  $2_1^+$  transition in  $^{182,184}\text{Hg}$  is a strong fingerprint of shape coexistence as strong  $E0$  transitions are the result of considerable mixing of two states with a large difference in deformation [29]. Combining the measured conversion coefficients with the re-evaluated  $B(E2)$  values from the Coulomb excitation experiments [2] will result in  $E0$  transition strength  $\rho^2(E0)$  values which can be compared with different theoretical models [30].

## 5. Conclusion

The low-lying excited states in  $^{182,184}\text{Hg}$  have been investigated following the  $\beta$  decay of  $^{182,184}\text{Tl}$ . The decay schemes of these nuclei have been extended and revised based on high-quality  $\gamma$ - $\gamma$  coincidence data. The detailed level scheme of the lowest energy states in  $^{182,184}\text{Hg}$  and the precise description of their decay properties (energy of the transitions, intensity and conversion coefficients), which were achieved in this analysis, provided crucial information for the re-evaluation of the  $^{182,184}\text{Hg}$  Coulomb excitation study performed at REX-ISOLDE with the Miniball setup [30].

## Acknowledgments

We thank the ISOLDE collaboration for providing excellent beams and the GSI Target Group for manufacturing the carbon foils. This work was supported by the European Commission through the Marie Curie individual fellowship program (FP7-PEOPLE-2009-IEF—252951—SHAPEXPIUM) and through I3-ENSAR (Contract No. RII3-CT-2010-262010) within the Seventh Framework Programme; by FWO-Vlaanderen (Belgium), by GOA/2010/010 (BOF KULeuven), by the IAP Belgian Science Policy (BriX network P6/23); by a grant from the European Research Council (ERC-2011-AdG-291561-HELIOS), by the United Kingdom

Science and Technology Facilities Council (STFC); by the Slovak grant agency VEGA (Contract Bo. 2/0105/11 1/0613/11); by the Slovak Research and Development Agency (Contract No. APVV-15-0225); and by the Reimei Foundation of Advanced Science Research Center (ASRC) of JAEA (Tokai, Japan).

## References

- [1] Heyde K and Wood J L 2011 *Rev. Mod. Phys.* **83** 1467
- [2] Bree N *et al* 2014 *Phys. Rev. Lett.* **112** 162701
- [3] Scheck M *et al* 2010 *Phys. Rev. C.* **81** 014310
- [4] Gaffney L M *et al* 2014 *Phys. Rev. C* **89** 024307
- [5] Elseviers J *et al* 2011 *Phys. Rev. C* **84** 034307
- [6] Marsh B *et al* unpublished
- [7] Andreyev A N *et al* 2003 *Eur. J. Phys. A* **18** 55
- [8] Bouldjedri A *et al* 1991 *Z. Phys. A* **339** 311
- [9] Keller J G *et al* 1986 *Nucl. Phys. A* **452** 173
- [10] Bolshakov V A *et al* 1993 *Proc. 6th Int. Conf. on Nuclei Far from Stability* ed A Woehr
- [11] Van Beveren C *et al* 2016 *J. Phys. G: Nucl. Part. Phys.* **43** 025102
- [12] Barzakh A *et al* 2017 *Phys. Rev. C* **95** 014324
- [13] Toth K S *et al* 1976 *Phys. Lett. B* **63** 150
- [14] Cole J D *et al* 1976 *Phys. Rev. Lett.* **37** 1185
- [15] Andreyev A N *et al* 2003 *Eur. J. Phys. A* **18** 39
- [16] Van Beveren C *et al* 2015 *Phys. Rev. C* **92** 014325
- [17] Fedosseyev V N *et al* 2000 *Hyperfine Interact.* **127** 409
- [18] Elseviers J *et al* 2013 *Phys. Rev. C* **88** 044321
- [19] Bindra K S *et al* 1995 *Phys. Rev. C* **51** 401
- [20] Singh B 2015 *Nucl. Data Sheets* **130** 21
- [21] Audi G *et al* 2012 *Chin. Phys. C* **36** 1157
- [22] Kibédi T *et al* 2008 *Nucl. Instrum. Methods A* **589** 202
- [23] Ma W C *et al* 1984 *Phys. Lett. B* **139** 276
- [24] Wauters J *et al* 1994 *Phys. Rev. C* **50** 2768
- [25] Baglin C M 2010 *Nucl. Data Sheets* **111** 275
- [26] Delaroche J P *et al* 1994 *Phys. Rev. C* **50** 2332
- [27] Deng J K *et al* 1995 *Phys. Rev. C* **52** 595
- [28] Sferrazza M *et al* 1995 *Z. Phys. A* **353** 5
- [29] Wood L W *et al* 1999 *Nucl. Phys. A* **651** 323
- [30] Wrzosek-Lipska K *et al* 2017 Electromagnetic properties of low-lying states in neutron-deficient Hg isotopes: Coulomb excitation of  $^{182}\text{Hg}$ ,  $^{184}\text{Hg}$ ,  $^{186}\text{Hg}$  and  $^{188}\text{Hg}$  (in preparation)
- [31] Baglin C M 2003 *Nucl. Data Sheets* **99** 1